Effect of Magnetic Doping on the Electronic States of Ni

K. N. Altmann,[1] N. Gilman,[2] J. Hayoz,[2] R. F. Willis,[2] and F. J. Himpsel[1]

[1]*Department of Physics, University of Wisconsin Madison, 1150 University Avenue, Madison, Wisconsin 53706-1390*
[2]*Department of Physics, Penn State University, University Park, Pennsylvania 16802-6300*
(Received 22 November 2000; published 4 September 2001)

Angle-resolved photoemission is used to determine the change in the electronic states of Ni induced by doping with Fe and Cr. Well-defined spin and **k** states are selected using high energy and **k** resolution combined with single crystal alloys. Iron suppresses the mean free path of minority spins only, while chromium suppresses both spins and decreases the magnetic splitting. The strong variation of these effects from one impurity to the other supports the concept of magnetic doping.

Magnetoelectronics is a rapidly developing field of electronics where spin currents replace charge currents [1]. The central goal of magnetoelectronics is the generation and switching of spin currents. The spin-dependent current density $\mathbf{j} = \sigma \mathbf{E}$ in an electric field $\mathbf{E}$ is controlled by the conductivity $\sigma = (e^2/m)n\tau$ for the two spin directions. It is determined by the carrier density n and their lifetime τ, which is related to the mean free path l and the Fermi velocity v_F via $\tau = l/v_F$. As in semiconductor electronics, one may introduce the idea of doping. The analogs of acceptors and donors are spin-polarized impurities that shift the balance towards spin up or spin down carriers. In addition to manipulating the carrier density n there is the option of affecting the mean free path l by spin–selective scattering.

Transport measurements suggest that magnetic impurities can influence the mean free path of carriers and thereby create spin polarization [2,3]. Parallel and antiparallel combinations of spin filters generate giant magnetoresistance (GMR), a phenomenon utilized widely in magnetoelectronics. Two equal filters give rise to the ordinary GMR effect, where the resistance decreases from the antiparallel to the parallel orientation. Two different filters, however, can exhibit an inverse GMR effect where the resistance increases [4,5]. It occurs when one of the filters selects majority spins, the other minority spins. An example is the combination of a Fe layer with a Fe/Cr multilayer [4]. Adding Cr in the multilayer favors minority spins, whereas the pure Fe layer transmits mainly majority spins. A similar effect is observed in Fe doped with V [5]. Such an explanation is consistent with the ratio of the majority and minority spin resistivities derived from ternary alloys [2]. It is suggestive to connect selective spin scattering with the magnetic orientation of such impurities [6]. Dopants with parallel orientation tend to favor majority spins and vice versa. Another type of magnetic doping has been detected at interfaces of magnetic materials, where the spin-dependent reflectivity and magnetoresistance can be affected by submonolayer amounts of magnetic materials [7].

Magnetoresistance measurements of multilayer structures and resistivity measurements on ternary alloys have provided estimates for the spin-dependent mean free path within certain models [2–5]. However, relatively little is known about the microscopic mechanism that causes the spin dependence. In order to have the maximum impact on the theory of electronic states in these alloys, measurements are needed that resolve a specific state at a well-defined energy E and momentum $\hbar\mathbf{k}$. Angle-resolved photoemission is now able to resolve states within thermal energies $k_B T$ around the Fermi level E_F ($k_B T = 17$ meV at the measurement temperature of 200 K). The momentum resolution has improved such that the spin-dependent mean free path l can be determined from the momentum broadening δk via the uncertainty relation $l = 1/\delta k$ [8,9]. The other two parameters in σ can be probed as well, $v_F = \hbar^{-1}\partial E/\partial \mathbf{k}$ via the slope of $E(\mathbf{k})$ and n via the peak areas. We combine these advances with the use of highly perfect single crystals of alloys to obtain state- and spin-specific mean free paths. The results vary strongly with the concentration of the impurity, and they differ between Fe and Cr as dopant. Such observations suggest that magnetic doping is a viable concept and provides critical input for a microscopic understanding of the effect.

The samples were single crystals of Ni(110), $Ni_{0.9}Fe_{0.1}$(110), $Ni_{0.8}Fe_{0.2}$(110), and Ni(110) with variable amounts of Cr diffused into it. Although these alloy single crystals were cumbersome to prepare to perfection, they allowed us to obtain much sharper features at E_F than epitaxial thin films (compare [8,10]). Films cannot be annealed high enough because of interdiffusion with the substrate, which begins at about 200 °C on Cu and at about 500 °C on Ni. The preparation of single crystals involved removal of bulk impurities by annealing in 100 Torr H_2 over a period of several days with the temperature ramping up from 500 to 850 °C, removal of segregated impurities by repolishing, electropolishing in a chromic acid solution [11], and sputter annealing with anneals up to 800 °C.

The stoichiometry was determined *in situ* by taking the areas of the $3p$ core level peaks at a photon energy $h\nu = 170$ eV and including minor corrections for the cross section and for the energy-dependent transmission of the spectrometer. Thereby, the stoichiometry and the electronics states were sampled over a comparable probing

depth. For the Ni-Fe alloys the stoichiometry came out to be equal to that of the bulk, confirming that segregation effects were small [12]. For Cr doping we evaporated 8 Å of Cr into a pure Ni(110) surface and diffused the Cr into the Ni crystal at temperatures of 650–700 °C until the desired stoichiometry was reached. That implies a diffusion length of about 80 Å for a typical Cr concentration of 10%. The resulting concentration gradient within the probing depth of 5–10 Å is negligible.

Photoemission spectra were obtained using an electron spectrometer with energy and angle multidetection, together with p-polarized synchrotron radiation from an undulator. The detection geometry was optimized for minimizing interference with other bands near E_F and for minimizing the $k^\perp$ broadening that is caused by the finite probing depth. This is achieved by having $k^\perp$ tangent to the Fermi surface along the $[\bar{1}10]$ symmetry line, such that the variation of the Fermi level crossing with $k^\perp$

vanishes to first order. Details of the band structure and Fermi surface can be found in [9], Figs. 1 and 4.

As is typical for the states that dominate magnetic transport properties we select the Σ_1 band which has both s, p, and d character (Figs. 1 and 2). It combines a substantial group velocity ($v_f = 0.28 \times 10^6$ m/s) with magnetic splitting. It is also nearly isotropic, which makes it characteristic for a large part of the Fermi surface. Theoretical models of ferromagnets have frequently used such a band. Additional data from pure d states near the X point exhibit features similar to the Σ_1 band, such as a decrease of the minority spin peak for Fe doping (Fig. 3). The selected Σ_1 band crosses E_F along the $[\bar{1}10]$ azimuth at a photon energy $h\nu = 27$ eV for the (110) surface. It starts out at the Γ_{12} point in the 2nd Brillouin zone at $k^\parallel = 2.52$ Å, disperses up across E_F towards the K point, and eventually reaches the X point at $k^\parallel = 0$. In Fig. 1 the value of $k^\parallel$ is reduced to the 1st Brillouin zone, i.e., the experimental $k^\parallel$ is subtracted from 2.52 Å.

The spectra shown in Fig. 1 represent not the usual energy distribution, but the momentum distribution with the energy fixed at $E_F \pm 10$ meV. Thereby we focus onto the states within kT of E_F that are responsible for carrying charge and spin currents. For clean Ni(110) we observe two well-resolved peaks in Fig. 1 that are assigned to the majority and minority spin component of the Σ_1 band (arrows). For pure Ni such an assignment is obvious from the calculated band topology (see [9] and Fig. 2). For the alloys we can clearly track the peaks towards zero impurity concentration and infer their spin from that. However, we caution that there is the possibility that the spin polarization of the two bands might be reduced from 100% by alloying. Nevertheless, one can argue that the band with the larger Fermi wave vector has higher filling and, therefore, is the majority spin band.
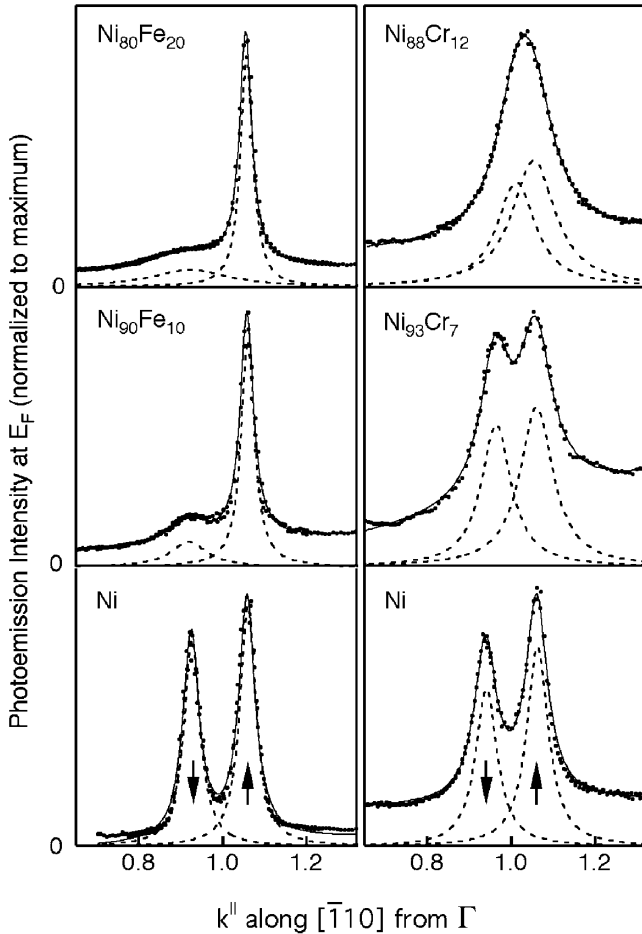

FIG. 1.   Effect of magnetic doping on the Σ_1 conduction band of Ni(110) at $h\nu = 27$ eV. The momentum distribution of the spin down peak broadens rapidly with increasing Fe concentration (left), due to a decrease in the mean free path $l_\downarrow$. Both peaks become broader with Cr doping (right), showing that Cr scatters both spins.
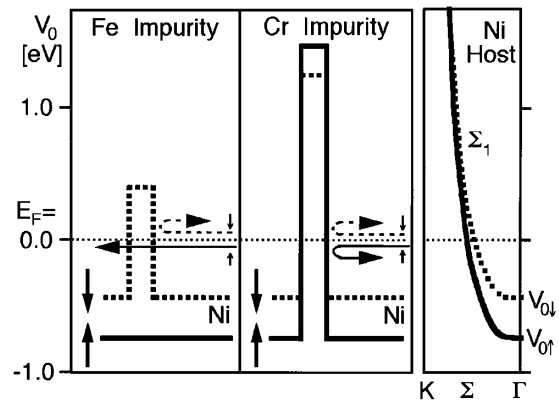

FIG. 2.   Schematic of the potential barriers induced by Fe and Cr impurities in Ni, based on the local potential V_0 for the two spins. V_0 is obtained from the minimum of the Σ_1 band along the [110] direction $\Gamma\Sigma K$ in fcc Ni, Fe, Cr. Spin-dependent barriers lead to spin-selective, elastic scattering [15].
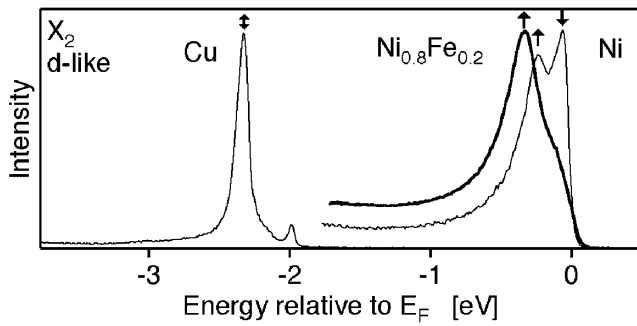
FIG. 3. Effect of Fe doping on the d band of Ni(110) at $h\nu = 15$ eV, $k^{\parallel} = 0$ (X_2 point). The spin down peak is quenched in the energy distribution.

Each spectrum provides four numbers that are fundamental to spin transport in an alloy. The widths $\delta k_{\uparrow}, \delta k_{\downarrow}$ of the two spin peaks provide the mean free paths $l_{\uparrow}, l_{\downarrow}$ and the Fermi wave vectors $k_{F\uparrow}, k_{F\downarrow}$ determine the band filling. The magnetic splitting $\delta k_{ex} = k_{F\uparrow} - k_{F\downarrow}$ is a qualitative measure of the difference in band filling, i.e., the magnetic moment. The calculation of the mean free path is a straightforward application of the uncertainty relation. An exponentially decaying wave function $\psi(x)$ whose probability density $\psi^{*}\psi$ decays with length l gives a Lorentzian for the probability density $\Psi^{*}\Psi$ of its Fourier transform $\Psi(k)$. The full width half maximum is $\delta k = 1/l$. Indeed, we find that the momentum distributions in Fig. 1 can be fitted by Lorentzians plus a linear background, which represents diffusely scattered electrons. The results compiled in Table I provide lower limits of the mean free paths $l_{\uparrow}$ and $l_{\downarrow}$ since we have not subtracted momentum broadening by phonon scattering, residual $k^{\perp}$ broadening, sample imperfections, and instrumentation. For example, transport measurements give $l_{\uparrow} = 46$ Å for Ni$_{0.8}$Fe$_{0.2}$ at room temperature [13]. For a mean free path shorter than 20 Å the corrections become small, and our values compare well to transport measurements, e.g., $l_{\downarrow} \leq 6$ Å for Ni$_{0.8}$Fe$_{0.2}$ [13].

TABLE I. Magnetic splitting δk_{ex}, full width half maximum $\delta k_{\uparrow}$, $\delta k_{\downarrow}$, and mean free path $l_{\uparrow}, l_{\downarrow}$ for NiFe and NiCr alloys (± 0.01 Å^{-1}).

	δk_{ex} [Å^{-1}]	$\delta k_{\uparrow}$ [Å^{-1}]	$\delta k_{\downarrow}$ [Å^{-1}]	$l_{\uparrow}$ [Å]	$l_{\downarrow}$ [Å]
Ni	0.14	0.046[a]	0.046[a]	>22	>22
Ni$_{0.9}$Fe$_{0.1}$	0.14	0.04[a]	0.10	>25	10
Ni$_{0.8}$Fe$_{0.2}$	0.14	0.03[a]	0.22	>33	5
Ni[b]	0.12	0.062[a]	0.062[a]		
Ni$_{0.93}$Cr$_{0.07}$	0.09	0.096	0.086	11	10
Ni$_{0.88}$Cr$_{0.12}$	≤ 0.05	0.12	0.11	8	9

[a]Peak broadened by sample imperfections and finite momentum resolution.
[b]The Ni crystal used for the Cr deposition (Fig. 1, right) was different from the Ni crystal in Fig. 1, left. The peaks are broader and the splitting is smaller, which could be due to Cr contamination.

The data reveal several trends. In Fe-doped Ni only the minority peak is broadened. Its width $\delta k_{\downarrow}$ is roughly proportional to the Fe concentration x, i.e., the mean free path $l_{\downarrow}$ decreases like $1/x$. In Cr-doped Ni both peaks are broadened, with $\delta k_{\uparrow}$ slightly larger than $\delta k_{\downarrow}$ and both comparable to the $\delta k_{\downarrow}$ for Fe doping. These results clearly demonstrate the existence of spin-selective scattering induced by an impurity, which will contribute to spin-dependent transport. The area ratio of minority/majority spins decreases by a factor of 2–3 with Fe impurities, reinforcing the concept of spin selection by dopants. That is also true for the d states in Fig. 3. A possible explanation would be a transfer of spectral weight from the Σ_1 band of Ni to separate impurity levels above E_F. As indicated in Fig. 2, such levels can be expected for minority spins at a Fe site, and for both spins on Cr sites. The magnetic splitting does not change significantly for the Fe concentrations considered here, but decreases with Cr doping, tracking the decreasing magnetic moment. δk_{ex} reaches zero at a Cr concentration close to 13% where NiCr alloys become paramagnetic. For 12% Cr a two line fit has been used in analogy to the other concentrations, but a single line fit would also have been consistent with the data. The decrease of δk_{ex} is primarily due to $k_{F\downarrow}$ moving towards a stationary $k_{F\uparrow}$, as in pure Ni close to the Curie temperature [14].

For explaining the observed spin-selective scattering one can distinguish elastic and inelastic processes. The discontinuity of the potential V_0 at an impurity generates a barrier (Fig. 2) which gives rise to elastic scattering of Bloch waves [15]. The change of V_0 occurs over the screening length, which is comparable to an atomic distance in metals. In order to estimate the jump in V_0 we have used the bottom of the Σ_1 band that underlies our study (right side of Fig. 2 and [16]). Near a Fe impurity, the majority spin potential is very close to its counterpart in the Ni host, but the minority spin potential is significantly higher due to the larger magnetic splitting. Therefore, only the minority states see a scattering potential at a Fe impurity. For Cr, both spins experience a potential barrier since the reduced number of d electrons in Cr shifts the states up relative to E_F. The discontinuity is somewhat larger for spin up states due to the antiferromagnetic orientation of Cr in Ni. This model suggests a strategy for selecting hosts and dopants that boosts minority spin currents via a longer mean free path: Align the minority spin bands by choosing a host with a large ferromagnetic splitting, such as Fe and Co, and a dopant with lower band filling. Indeed, such systems exhibit inverse GMR [4,5] and resistivity ratios [2] $\alpha = \rho_{\downarrow}/\rho_{\uparrow} < 1$.

A typical inelastic process is the creation of an electron-hole pair near the Fermi level E_F. This process approximately conserves spin. An impurity that introduces minority spin states near E_F will selectively scatter minority spins and vice versa. For inelastic scattering we have to consider not only the conduction band shown in Fig. 2, but also several d bands. In fcc Ni and Fe the majority

spin d bands lie all below E_F, which leaves minority spin d bands as scatterers at E_F. In fcc Cr, however, d bands with both spins occur at E_F, which qualitatively explains the observed trend. The changes of the available scattering states with doping can be quantified by detailed measurements of the Fermi surfaces of magnetic alloys [10].

In summary, we observe a strong effect of magnetic impurities on the electronic states of Ni near the Fermi level, where they are relevant to magnetoelectronics. The mean free path, magnetic splitting, and carrier density are affected by Fe and Cr concentrations of a few percent only. The changes depend on the impurity, suggesting that there are opportunities for tailoring spin transport by magnetic doping. In particular, spin-selective scattering is able to affect the balance of spin currents. However, the simple expectation that Cr and Fe act exactly opposite because of their opposite spin orientation is not realized. Fe affects mainly minority spins, whereas Cr affects both spins. Highly resolved photoemission data from specific bands at specific **k** points, such as those demonstrated here, provide a critical test for developing a microscopic theory of spin-dependent scattering in magnetoelectronics [15,17].

Note added.— Recently, the band structure of NiFe alloys was calculated from first principles, including the photoemission spectra and the k broadening due to spin-dependent scattering [18]. The results match our data in Fig. 1 quite well and thereby support a spin-dependent potential barrier, such as shown in Fig. 2.

[1] G. A. Prinz, J. Magn. Magn. Mater. **200**, 57 (1999).

[2] A. Fert and I. A. Campbell, J. Phys. F **6**, 849 (1976); I. A. Campbell and A. Fert, in *Ferromagnetic Materials,* edited by E. P. Wohlfarth (North-Holland, Amsterdam, 1982), Chap. 9, p. 747.

[3] J. Bass, W. R. Pratt, and P. A. Schroeder, Comments Condens. Matter Phys. **18**, 228 (1998); J. Bass and W. Pratt, J. Magn. Magn. Mater. **200**, 274 (199); W. Park, R. Loloee, J. A. Caballero, W. P. Pratt, P. A. Schroeder, J. Bass, A. Fert, and C. Vouille, J. Appl. Phys. **85**, 4542 (1999).

[4] J. M. George, L. G. Pereira, F. Petroff, L. Steren, J. L. Duvail, and A. Fert, Phys. Rev. Lett. **72**, 408 (1994).

[5] S. Y. Hsu, A. Barthélémy, P. Holody, R. Loloee, P. A. Schroeder, and A. Fert, Phys. Rev. Lett. **78**, 2652 (1997).

[6] S. Blügel, H. Akai, R. Zeller, and P. H. Dederichs, Phys. Rev. B **35**, 3271 (1987); R. Zeller, J. Phys. F **17**, 2123 (1987), and references therein.

[7] S. S. P. Parkin, Appl. Phys. Lett. **61**, 1358 (1992); Phys. Rev. Lett. **71**, 1641 (1993).

[8] D. Y. Petrovykh, K. N. Altmann, H. Höchst, M. Laubscher, S. Maat, G. J. Mankey, and F. J. Himpsel, Appl. Phys. Lett. **73**, 3459 (1998).

[9] F. J. Himpsel, K. N. Altmann, G. J. Mankey, J. E. Ortega, and D. Y. Petrovykh, J. Magn. Magn. Mater. **200**, 456 (1999).

[10] F. O. Schumann, R. F. Willis, K. G. Goodman, and J. G. Tobin, Phys. Rev. Lett. **79**, 5166 (1997); M. Hachstrasser, N. Gilman, R. F. Willis, F. O. Schumann, J. G. Tobin, and E. Rotenberg, Phys. Rev. B **60**, 17 030 (1999); N. Gilman *et al.* (to be published).

[11] F. Schedin, L. Hewitt, P. Morrall, V. N. Petrov, and G. Thorton, Phys. Rev. B **61**, 8932 (2000).

[12] R. G. Jordan, M. A. Hoyand, and E. A. Seddon, J. Phys. Condens. Matter. **2**, 779 (1990).

[13] B. A. Gurney, V. S. Speriosu, J. P. Nozieres, H. Lefakis, D. R. Wilhoit, and O. U. Need, Phys. Rev. Lett. **71**, 4023 (1993).

[14] P. Aebi, T. J. Kreutz, J. Osterwalder, R. Fasel, P. Schwaller, and L. Schlapbach, Phys. Rev. Lett. **76**, 1150 (1996); T. J. Kreutz, T. Greber, P. Aebi, and J. Osterwalder, Phys. Rev. B **58**, 1300 (1998).

[15] W. H. Butler, X. G. Zhang, D. M. C. Nicholson, and J. M. MacLaren, J. Magn. Magn. Mater. **151**, 354 (1995).

[16] The values of V_0 in Fig. 2 are based on inverse photoemission data and calculations for the bottom of the Σ_1 band (Γ_{12}) in fcc Ni, Fe, and Cr. The spin average of V_0 is determined by the band filling, i.e., the atomic number. The spin splitting of V_0 is roughly proportional to the magnetic moment (≈ 1 eV$/\mu_B$), which is $+2.7$ μ_B for Fe in Ni and -0.2 μ_B for Cr in Ni [6]. See F. J. Himpsel, Phys. Rev. Lett. **67**, 2363 (1991); H. Glatzel, R. Schneider, T. Fauster, and V. Dose, Z. Phys. B **88**, 53 (1992); G. J. Mankey, R. F. Willis, and F. J. Himpsel, Phys. Rev. B **48**, 10 284 (1993); G. Y. Guo and H. H. Wang, Phys. Rev. B **62**, 5136 (2000).

[17] Ph. Lambin and F. Herman, Phys. Rev. B **30**, 6903 (1984); D. M. C. Nicholson, W. H. Butler, W. A. Shelton, Y. Wang, X.-G. Zhang, and G. M. Stocks, J. Appl. Phys. **81**, 4023 (1997); A. E. Krasovskii, Phys. Rev. B **60**, 12 788 (1999); I. I. Mazin, Phys. Rev. Lett. **83**, 1427 (1999).

[18] P. E. Mijnarends, S. Sahrakorpi, M. Lindroos, and A. Bansil, Phys. Rev. B (to be published).